Available online at www.sciencedirect.com
SCIENCE DIRECT®
Combustion and Flame 142 (2005) 413–427
Combustion and Flame
www.elsevier.com/locate/combustflame

Experimental and computational studies of oxidizer and fuel side addition of ethanol to opposed flow air/ethylene flames

Kevin L. McNesby [a,*], Andrzej W. Miziolek [a], Thuvan Nguyen [a], Frank C. Delucia [a], R. Reed Skaggs [a], Thomas A. Litzinger [b]

[a] *Army Research Laboratory, Aberdeen Proving Ground, MD 21005-5066, USA*
[b] *Penn State University, State College, PA, USA*

Received 20 May 2004; received in revised form 1 April 2005; accepted 12 April 2005

Available online 5 July 2005

Abstract

Results of computations based on a detailed chemical kinetic combustion mechanism and results of experiments are compared to understand the influence of ethanol vapor addition upon soot formation and OH radical concentration in opposed flow ethylene/air diffusion flames. For this work, ethanol vapor was added to either the fuel or the oxidizer gases. Experiment and calculations are in qualitative agreement, and both show differing concentrations of soot, soot precursors, and OH depending on whether the ethanol is added to the fuel or oxidizer gases. An explanation for the observed differences for oxidizer or fuel side ethanol addition to opposed flow ethylene/air diffusion flames is proposed, based on an analysis of the chemical kinetic mechanism used in the computations.
© 2005 Published by Elsevier Inc. on behalf of The Combustion Institute.

Keywords: Soot formation; Opposed flow flames; Ethylene flames; Ethanol; PLIF

1. Introduction

It is estimated that U.S. military aircraft emit about 600,000 kg of particulate matter into the atmosphere each year. Most of this particulate matter is in the form of soot particles with diameters less than 2.5 μm (PM2.5) [1]. In addition to shortening engine life and limiting the time between engine servicing, there is a growing body of evidence that shows these small particles cause both health and environmental problems [2–4].

As part of a Strategic Environmental Research and Development Program (SERDP) effort investigating superefficient (ppm level) fuel additives for soot reduction in turbine engines [5], fundamental studies of the effects of additives on soot formation and oxidation in different types of burners and combustors are underway at several laboratories using a wide range of diagnostic methods. Part of the rationale of this program is to use different types of burners and combustors (diffusion, premixed, well-stirred reactors, etc.) to approximate the different stages of fuel combustion that occur in a turbine engine. For the initial series of experiments for this program, ethylene was chosen as the fuel because it has been used in past studies of soot formation processes in a wide range of burners [6].

* Corresponding author. Fax: +1 410 306 1909.
E-mail address: mcnesby@arl.army.mil (K.L. McNesby).

0010-2180/$ – see front matter © 2005 Published by Elsevier Inc. on behalf of The Combustion Institute.
doi:10.1016/j.combustflame.2005.04.003

The part of the effort conducted at the Army Research Laboratory (ARL) uses an opposed flow burner to investigate ethylene/air combustion.

Soot reducing additives studied in the past largely fall into two categories, metal-based additives and oxygenated compounds [6]. Although often very effective at soot reduction, the investigation of metal additives was ruled out due to concerns about adverse health and environmental impact as well as incompatibility with gas turbines. Thus, the use of oxygenated compounds (that are drawing increasing attention for use in diesel engines) was selected [7]. It is worthwhile to note that oxygenated compounds are not seen as an ultimate solution to the particulate emission problem for gas turbine engines, because for noticeable effect they must be added at high concentrations (percentage levels) to the fuel [7], making them impractical. However, they do provide a good benchmark for the standardization tests. After considering the available data in the literature and compatibility with tests using ethylene, ethanol was selected as the initial additive compound to be studied [8,9]. The choice of ethanol and ethylene also allowed chemical mechanisms from the literature to be used in modeling of the results [10].

2. Background

The separation of the regions of highest particulate and aromatic concentrations (sooting region) and the main combustion (flame radical production) region in opposed flow flames has been reported in Ref. [11]. We are aware of only one investigator using simultaneous planar laser-induced fluorescence (PLIF) and light-scattering measurements in sooting opposed flow diffusion flames [12]. Simultaneous measurement has been reported in the literature for coflowing diffusion flames [13]. For sooting opposed flow flames, peak soot concentration typically occurs near the stagnation plane, in fuel-rich regions at temperatures slightly lower than peak combustion temperatures [14]. For opposed flow diffusion flames in which the stagnation plane is fuel rich (e.g., the flame reported here), the flame occurs at the location where fuel and oxidizer are close to stoichiometric combustion proportions. This occurs on the oxidizer side of the stagnation plane (see Fig. 1a), and the stoichiometric mixture is achieved by fuel gases diffusing upstream into the oxidizer flow. For the flames used here (ethylene/air) the overall chemical reaction (assuming air to be 20% oxygen) is

$$C_2H_4 + 3O_2 + 12N_2 \rightarrow 2CO_2 + 2H_2O + 12N_2. \quad \text{(R1)}$$

Reaction 1 (R1) shows that for fuel (C_2H_4) and oxidizer (air) flow rates that are approximately equal,

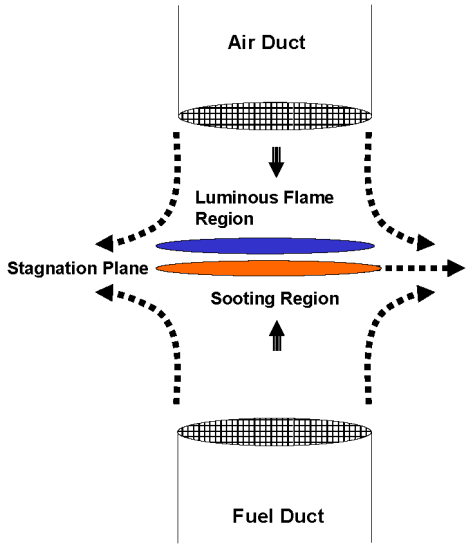

Fig. 1. A schematic of the opposed flow burner and flame.

in an opposed flow burner (our conditions), assuming gases with similar momenta (our conditions), the gas mixture at the stagnation plane will be fuel rich [14]. The stagnation plane is conceptually shown in Fig. 1. The stagnation plane is typically described as the location between the gas and the oxidizer ducts where the axial gas velocity goes to zero. For these experiments, the stagnation plane location was not measured, but was estimated by calculation.

For opposed flow flames that exhibit similar separations of sooting (particle laden) and flame (i.e., luminous) regions (e.g., ethylene/air, propane/air, heptane/air in the authors' experience), the effect of additives upon flame structure, radical formation, and extinction strain rate may be different depending on whether the additive is added to the fuel or oxidizer stream. As an example, when iron pentacarbonyl ($Fe(CO)_5$) is added to the air stream of many opposed flow hydrocarbon/air flame systems, it is among the most efficient flame inhibitors known. For fuel stream addition, the effect, on a molar basis, is much less pronounced [15].

The analysis of the experimental work described here attempts to understand the effect of fuel or air side addition of ethanol upon soot formation and OH radical concentrations in opposed flow ethylene/air flames. The approach focuses on a comparison of experimental results with results of flame modeling calculations incorporating the well-characterized C_2 combustion mechanism of Frenklach and coworkers [10]. This mechanism was developed for premixed flame systems, and we have used it here without modification. It may be worth noting that the activation energies for some reactions in the mechanism may exhibit a pressure dependence in ethyl-

ene/air counterflow flames [16]. As noted above, the experiments take advantage of the spatial separation between regions of peak soot (particles) and OH concentrations in the opposed flow ethylene/air flames. This spatial separation allows a single laser pulse, tuned to resonance with an OH absorption, to be used to simultaneously measure OH laser-induced fluorescence (LIF) and light scattering (Mie + Rayleigh) by soot particles.

3. Experimental conditions

The opposed flow burner is constructed of 304 stainless steel, and is based on the design of Lentati and Chelliah [17]. Fuel (ethylene) and oxidizer (air) ducts are 15 mm in diameter, and are separated by 10 mm. Flow rates for the experiments reported here were 4.6 L/min ethylene and 6.2 L/min air. These values were chosen because they gave the most stable flame. Ethanol vapor was added to fuel or oxidizer gases using an injection pump (Isco). The ethanol was injected as a liquid at room temperature into the fuel or oxidizer gas lines approximately 2 m upstream from the gas entrance into the burner assembly and was assumed to vaporize completely. Ethanol addition was up to 0.08 mol fraction (8%) in the fuel or oxidizer gas stream. It should be noted that this level (8%) of addition to the oxidizer stream makes the "oxidizer" a rich fuel/air mixture. The change in flame behavior as the oxidizer gas stream is transitioned to a fuel/air mixture is treated in detail in what follows. A shroud gas (nitrogen) surrounded both fuel and oxidizer ducts within the burner assembly to minimize entrainment of room air into the flame. The burner was enclosed in a chamber that was capable of being evacuated. However, for these experiments the access ports of the chamber were left open and so all experiments were run at atmospheric pressure. A schematic of the experimental apparatus is shown in Fig. 2.

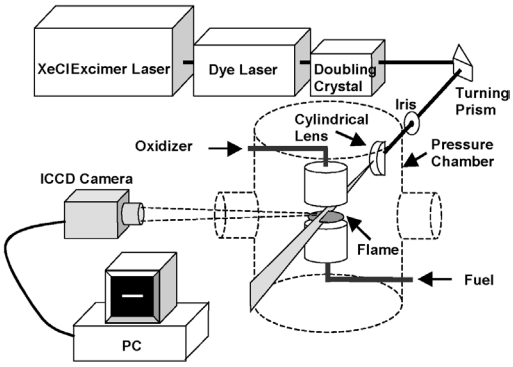

Fig. 2. A schematic of the experimental apparatus.

The experimental procedure was as follows. A flame source was placed between the burner ducts and gas flow was then commenced, with the opposed flow flame igniting immediately. The nitrogen shroud gas flow (5 L/min total) was initiated and the flame was allowed to stabilize for 5 min. For experiments using fuel or oxidizer additive, a valve on the injection pump was opened and flow of ethanol into the air or ethylene streams was begun. After approximately 1 min of flow of ethanol, a sheet of pulsed laser radiation (typically 0.5 mJ/pulse, approx 20-ns duration, formed using a double apertured, half-cylindrical lens) near a wavelength of 281 nm (Lambda Physik Excimer/Scanmate system: Coumarin 153 dye; Fundamental at 560 nm, 2× frequency to 281 nm; pump $A^2\Sigma^+$ $(v = 1) \leftarrow X^2\Pi$ $(v = 0)$, detect ((0,0), (1,1) around 310 nm) was passed through the flame region. A gated, unfiltered, intensified CCD camera (Roper Scientific, 256 × 1024 pixels), equipped with a Nikor 1:4.5 UV lens, was used to measure laser scatter during and immediately following the laser pulse (camera gate width = 80 ns). The images produced by 100 laser pulses were averaged in the camera memory. From this average image, the maximum value at a given pixel location along the centerline between the fuel and the oxygen ducts was selected in the sooting and combustion regions of the flame (see Fig. 3). A background value at that pixel location, measured prior to the flame initiation (also 100 averaged images), was subtracted from this value. This background-corrected pixel value became the data point representing peak particle or OH concentration. Following data collection, the injection pump valve was closed, the pump flow parameters were reset, and the process repeated. Planar laser-induced fluorescence and light scatter measurements at the beginning and end of each run series were performed to check that the flame returned to normal after the ethanol

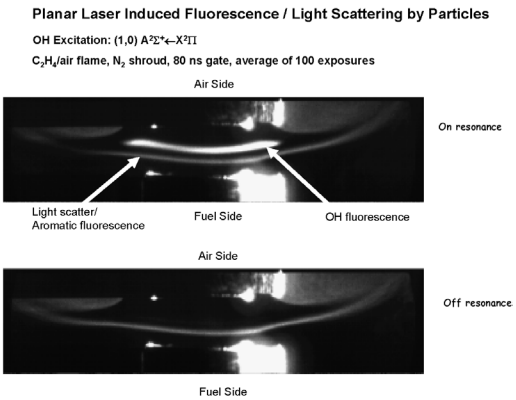

Fig. 3. (Upper) Simultaneous image of OH PLIF and light scattering by soot particles. (Lower) Same image, but with the laser tuned off of resonance with the OH absorption.

flow was stopped. Laser power was measured before and after each experimental run and typically varied by less than 2%. Other than subtraction of background, no corrections were made for changes in laser power or variations in spatial intensity, and no other specific dark field pixel corrections were made, although previous measurements of the CCD dark field (camera blocked) showed pixel to pixel output to vary by less than 2%.

The region of the flame referred to here as the sooting region (and other flame regions) may contain particles and polyaromatic hydrocarbons (PAH). These PAH are known to fluoresce when exposed to ultraviolet radiation [18]. For the experiments reported here, we are assuming that the bulk of the signal observed in the sooting region is from scattered laser radiation [19]. To evaluate the part of the observed image in the sooting region due to light scatter, we divided the theoretical treatment of the scattering process into an extinction part and a Mie theory part [20–22].

The intensity of scattered laser light (assuming unit incident intensity and zero absorption) by particles in the flame may be approximated by Bouguer's Law:

$$I = \exp(-3Q_e m_p L/2\rho d). \tag{2}$$

Here, I is the intensity of the scattered light, Q_e is the soot extinction coefficient, m_p is the weight of soot particles per unit volume, L is the pathlength, and ρ and d are the density and diameter of the average soot particle. This equation predicts that as soot particle size (d) decreases for a fixed soot mass per unit volume, scattering intensity increases.

According to Mie's solution of Maxwell's equations in spherical coordinates for an electromagnetic wave incident on a sphere [22], the angular distribution of intensity and degree of polarization of the light scattered by a collection of particles are related to both the size and index of refraction of the particles. The general solution describing scattering of monochromatic light by a single particle of any size may be described by

$$I_\theta = \lambda^2/(8R^2\pi^2)\big[i_1(\theta) + i_2(\theta)\big]. \tag{3}$$

Here, I_θ is the light intensity scattered at angle θ, λ is the wavelength of the incident radiation, R is the distance from the particle to the point of observation, and $i_1(\theta)$ and $i_2(\theta)$ are angular distribution intensity functions that are dependent on the intensities of the two plane polarized components of the scattered monochromatic incident light.

Application of Mie's solutions for light scattering by particles is usually simplified by considering the limiting cases where the particle diameter is much smaller than the wavelength of light (Rayleigh scattering, λ^{-4} intensity dependence), near the wavelength of light (Mie scattering), or much greater than the wavelength of light (diffractive optics). For light scattering by nascent soot particles in opposed flow flames (soot particle sizes of tens to hundreds of nanometers), the scattering is typically categorized as having characteristics of Rayleigh and Mie scattering. For observation at 90° to the incident beam, scattering in both Rayleigh and Mie regions is predicted to be perpendicularly polarized and nonzero.

So, for measurement of scattering intensity perpendicular to the incident laser beam, by a cloud of spherical particles with fixed size distribution, in the limit of $(3Q_e m_p L/2\rho d) \ll 1$, the scattering intensity should be approximately proportional to m_p, and hence to soot volume fraction.

Fig. 3 shows images of simultaneous light scattering and OH LIF taken perpendicular to the plane of the laser sheet. In this figure, the regions of maximum particle concentration and OH formation are seen to be well separated. Also shown in the figure is an image taken of the same flame with the laser tuned off of resonance with the OH absorption transition ((1,0) $A^2S \leftarrow X^2P$).

Calculations used the OPPDIF flow code, based on the Chemkin database, marketed by Reaction Design, Inc. The chemical mechanism input to the OPPDIF flow code used the Frenklach mechanism [10] for ethane combustion, modified by one of us (T.A.L.) to include ethanol addition. The final chemical mechanism incorporates 156 species and contains 659 reactions. Input conditions for the calculations assumed initial gas temperatures at 300 K, 1 atm total pressure, duct separation of 1 cm, and initial fuel and oxidizer gas stream velocities of 41 and 55 cm/s, respectively. For the burner system used in the experiments, the fuel velocity was approximately 41 cm/s, and the oxidizer velocity was approximately 55 cm/s. Duct separation was 1 cm. Each calculation required approximately 100 min to reach convergence on a Pentium 4-based desktop computer. The results of the Chemkin calculations predict flow parameters (gas velocity, strain, etc.), temperature, and species profiles as a function of distance from the fuel duct. The Frenklach mechanism allows prediction of species profiles for aromatic rings up to A4 ($C_{16}H_{10}$).

Two approaches were used for the calculations. In the first approach, the initial conditions input to the program specified a 60-point space grid between the burner ducts, with grid spacings becoming smaller near the combustion region. As the calculation proceeds, the program regrids to finer increments. When this initial grid was used, calculations often had difficulty converging, or took several hours to converge. The second approach used a 5-point, evenly spaced grid as the initial condition. The program was then al-

lowed to regrid as the calculation proceeded. In every case for which convergence was achieved, although final results for the two approaches agreed, the second approach converged faster. Convergence criteria used for Newton iteration and for time stepping were the program default values, with the exception of the cases of 5 to 8% ethanol added to the air stream. To achieve convergence for these cases, it was necessary to relax the convergence criteria by a factor of 100. This reduction was achieved by relaxing the default values for the absolute (ATOL) and relative convergence criteria (RTOL) for Newton iteration from default values of 10^{-9} and 10^{-4}, respectively, to 10^{-7} and 10^{-2}. The absolute (ATIM) and relative (RTIM) convergence criteria for time stepping were also relaxed from default values of 10^{-9} and 10^{-4}, respectively, to 10^{-7} and 10^{-2}. The final grid for these cases contained approximately 2/3 the number of grid points as for the other calculations (from 97 to 65). The calculated results for all cases are included here for completeness.

4. Results and discussion

4.1. Neat ethylene/air opposed flow flames

Fig. 4 shows a graph of calculated mole fraction profiles versus distance from the fuel duct for OH, C_2H_2, C_3H_3, A1 (benzene, C_6H_6), and A4 (pyrene, $C_{16}H_{10}$) for a neat ethylene/air opposed flow flame. Overlaid onto Fig. 4 are values of pixel intensity along the centerline between the burner ducts, measured using the light scattering/PLIF technique, for the same flame. The calculation is in reasonable agreement with observation. The calculation predicts the separation of regions of maximum soot concentration (assuming A1–A4 to be soot precursors in fuel-rich environments [23–25]) and OH. The experimental data in this figure have been background-corrected by subtracting the pixel dark current. To compare the data, the spatial location of the peak from OH fluorescence (relative to the fuel duct) measured in the flame was matched to the spatial location of the peak from OH predicted by the calculation. The measured light scatter from particles in the flame (and also possible broad band fluorescence from aromatics) is slightly closer to the fuel duct than the location of peak A1 and A4 concentrations predicted by the calculation. Because the soot particles in the flame are likely larger than A4, thermophoretic forces [26] may be driving the larger particles toward cooler regions of the flame. Also shown in Fig. 4 (dashed line) is an estimation of the location of the stagnation plane, based on the calculations. We have given the stagnation plane a finite width defined by the point where the axial gas velocity goes to zero (approximately 0.375 cm from the fuel duct) and the point where the radial gas velocity is at a maximum (approximately 0.428 cm from the fuel duct). The initial fuel and oxidizer gas stream velocities (for experiment and calculation) were 41 and 55 cm/s, respectively.

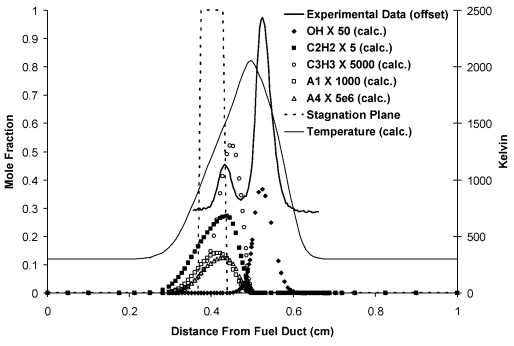

Fig. 4. Results of calculations showing temperature profile and separation of soot forming and flame radical regions for an undoped ethylene/air opposed flow flame, with overlay of measured centerline pixel intensities for similar flame. Also shown is estimated position of stagnation plane.

To understand how adding ethanol vapor to the fuel or oxidizer gases will affect the concentrations of OH and particles, we begin by identifying the main chemical reactions in our mechanism responsible for the conversion of ethylene to A1 (benzene) in neat opposed flow flames. The approach we used takes advantage of the postprocessor utility available in Chemkin that allows calculation of the rates of production and destruction of each species in the mechanism by each reaction involving that species. Fig. 5 shows the rate of production of A1 versus distance

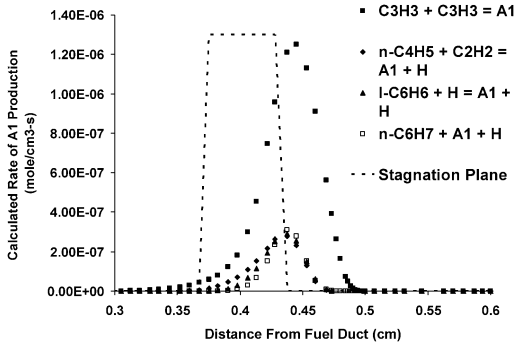

Fig. 5. The calculated rates of production of A1 versus distance from the fuel duct for the top four contributing reactions in the mechanism (out of 15 reactions in the mechanism involving A1). Calculation is for the neat ethylene/air opposed flow diffusion flame. Also shown is estimated position of stagnation plane.

from the fuel duct for the top four contributing reactions in the mechanism (out of 15 reactions in the mechanism involving A1). To assign a percentage contribution to A1 formation to each reaction, the area under the curve (divided by the local gas velocity) for each reaction was integrated, and this area per reaction compared to the area for the total rate of production for A1 (not shown in Fig. 5). According to this method, for A1 production in our neat ethylene/air opposed flow flame, the contribution of these four reactions is

$$C_3H_3 + C_3H_3 \rightarrow A1 \quad 73\%, \quad \text{(R4)}$$

$$n\text{-}C_4H_5 + C_2H_2 \rightarrow A1 + H \quad 12\%, \quad \text{(R5)}$$

$$l\text{-}C_6H_6 + H \rightarrow A1 + H \quad 8\%, \quad \text{(R6)}$$

$$n\text{-}C_6H_7 \rightarrow A1 + H \quad 6\%. \quad \text{(R7)}$$

It is worth noting that l-C_6H_6 and n-C_6H_7 are dependent upon reactions of n-C_4H_5 with acetylene. For radical species that are formed in one part(s) of the flame, and consumed in other parts of the flame, it is necessary to modify this approach by limiting the regions of integration.

This approach was used in the neat opposed flow ethylene/air flame to follow carbon as it passed from ethylene to A1. When the conversion from one species to another in the flame was near quantitative (such as the initial decomposition step of C_2H_4 to C_2H_3), tracing the reaction was straightforward. When the main path to A1 production was less than quantitative for destruction of a certain species (such as CH_2 conversion to C_3H_3), it was necessary to examine the contribution of all reactions to production and destruction rates for species participating in a given reaction. Using this method, the path to A1 from ethylene begins with the conversion of C_2H_4 to C_2H_3 (99%, via H and OH), followed by conversion of C_2H_3 to acetylene (C_2H_2) (90%). The formation of this acetylene "bath" is important to the chemistry of soot formation. However, as the initial ethylene/air mixture is fuel rich, approximately 44% of the acetylene formed in this step remains unreacted. The mechanism contains 77 reactions in which acetylene is a participant. Approximately 34% of the acetylene is converted to methylene (CH_2) and singlet methylene (CH_2^*), approximately 4% of which is converted to propargyl (C_3H_3), approximately 6% of which is converted to A1. Although propargyl is the main source of A1 formation, only a small fraction of propargyl reacts directly to form A1.

Table 1 shows the stepwise conversion of ethylene to A1 predicted by the calculation for this flame system, lists the reactions important for A1 formation, and some of the important competing reactions (where applicable) for steps leading to A1 production.

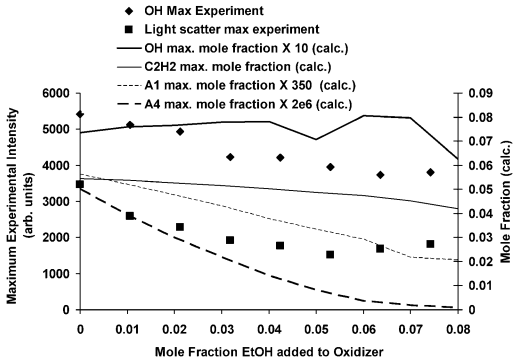

Fig. 6. Graph of experimental measurements and predictions based upon calculations for OH, soot, and soot precursors, for air side addition of ethanol.

Species in bold face in the reaction list on the right side of Table 1 are the species for which the rate of destruction listed applies. Also shown is the temperature at which maximum rates of destruction (ROD) and rates of production (ROP) for several species occur.

4.2. Oxidizer side addition of ethanol

In experiments and calculations, oxidizer side addition of ethanol vapor reduces soot and soot precursors. A graph of experimental measurements of peak light scatter and OH fluorescence and predictions of species maximum mole fraction based on calculations, for oxidizer side addition of ethanol, is shown in Fig. 6. The error in the measured scattered laser intensity and OH fluorescence is estimated to be approximately 5%, based upon pixel to pixel noise in the individual images. Overall, the change with increasing ethanol addition of calculated peak mole fractions for the species C_2H_2, A1, and A4 is in reasonable agreement with peak experimental values (measured along the centerline between burner ducts) of light scatter, while the change with increasing ethanol addition of the calculated peak mole fraction of OH is in average agreement with peak measured values of OH fluorescence, with calculation and experiment predicting a small decrease in peak OH concentration with ethanol addition. The slight increase in light scattering when ethanol vapor addition increases above 5% may be due to the transition from a diffusion flame to a partially premixed diffusion flame, and the onset of a secondary flame as the oxidizer mixture approaches premixed stoichiometry.

These results (decrease in soot, negligible change in peak OH concentration) at first seem contradictory. Soot reduction by addition of an oxygenated species is generally interpreted to be caused by an increase

Table 1
Reaction path of ethylene to A1 for neat ethylene/air opposed flow diffusion flames

Max. T (K) at peak		Neat ethylene/air opposed flow flame
ROP	ROD	
	1700	**C2H4**
		99% → **C2H3**
1700	1950	
		C2H3
		90% → **C2H2**
1700	2053	
		C2H2 → Unreacted (44%), **C2H2** → **C2H2** (18%), **C2H2** → **HCCO** (18%)
		HCCO → **CH2*** (87%)
2000	1950	**CH2*** → **CH2** (49%), **CH2** → **CH2*** (5%)
		CH2* → **C3H3** (4%)
1900	2000	**C3H3**
		4% → **A1** ↔ **A1-**
1550	1950	

C2H4 + H → C2H3 + H2 (91%)
C2H4 + OH → C2H3 + H2O (8%)

C2H3 (+M) → C2H2 + H (+M) (85%)
C2H3 + H → C2H2 + H2 (3.8%)
C2H3 + C2H2 → C4H4 + H (4%)
C2H3 + C2H4 → C4H6 + H (4%)

C2H2 + H → C2H + H2 (6.8%)
C2H2 + O → HCCO + H (18%)
C2H2 + O → CH2 + CO (18%)
C2H2 + C2H → C4H2 + H (9%)
C2H2 + OH → CH2CO + H (2%)
HCCO + H → CH2* + CO (87%)
HCCO + OH → C2O + H2O (13%)
CH2* + N2 → CH2 + N2 (34%)
CH2* + H2O → CH2 + H2O (15%)

CH2 + C2H2 → C3H3 + H (5%)
CH2* + C2H2 → C3H3 + H (4%)
CH2 + H → CH + H2 (82%)
CH2 + OH → CH2O + H (8%)
CH2 + OH → CH + H2O (4%)

C3H3 + C3H3 → A1 (4%)
C3H3 + OH → C2H3 + HCO (64%)
C3H3 + OH → C3H2 + H2O (31%)
C3H3 + CH2 → C4H4 + H (1%)

C3H3 + C3H3 → **A1** (71%)
n-C4H5 + C2H2 → **A1** + H (10%)
l-C6H6 + H → **A1** + H (10%)
n-C6H7 → **A1** + H (8%)

Note. Important reactions contributing to each species concentration are shown to the right. Percentage value in parenthesis refers to the amount of species in **bold** consumed or produced by that reaction.

in local OH radical [27] concentration, leading to increased soot oxidation:

$$C_xH_y\ (\text{soot}) + OH \rightarrow CO_2 + H_2O. \qquad (R8)$$

However, examination of the individual experimental images (Fig. 7) shows that as ethanol is added to the oxidizer (air) stream, the width of the OH region increases. We believe that the broadening of the OH region for this flame is the key to understanding the decrease in measured light scattering by particles. Figs. 8 and 9 show calculated temperature and OH mole fraction as a function of distance from the fuel duct. These figures show that the calculation predicts broadening of the OH and high-temperature flame regions with increasing oxidizer side ethanol addition. Fig. 10 shows the calculated rate of destruction of 4% ethanol vapor added to the oxidizer side of the opposed flow flame, overlaid with the calculated temperature profile for this flame and for the neat flame. The region of ethanol destruction is shown to coincide in location with the onset of the broadened region of high temperature in the flame to which ethanol has been added. We believe this broadened region of high temperature is indicative of a secondary flame zone as the oxidizer gas gradually changes to a fuel/air gas mixture.

Qualitatively, addition of ethanol vapor to the air stream causes the flame to change from a diffusion flame toward a partially premixed diffusion flame. The broadening of the OH region and of the tem-

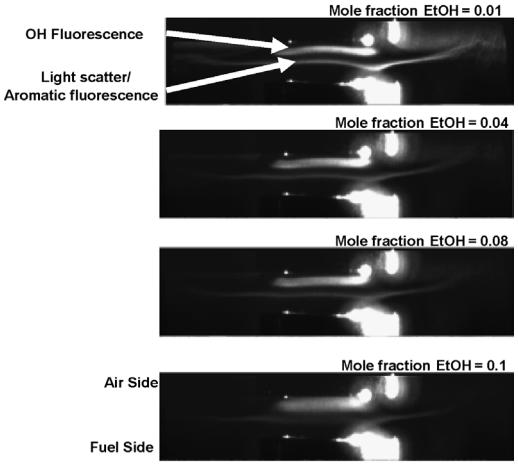

Fig. 7. Images of OH PLIF and light scattering by soot particles as increasing amounts of ethanol vapor are added to the air side. Note increasing width of OH region (upper feature) and decreasing intensity of light scatter from particles (lower feature).

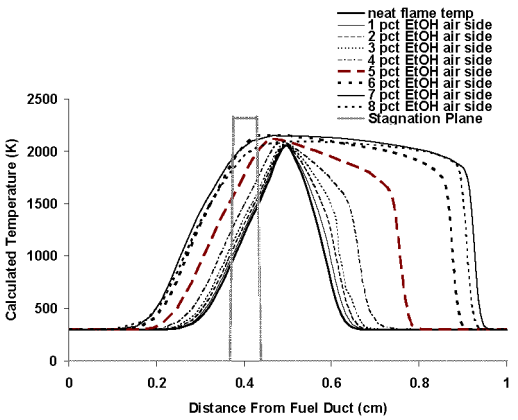

Fig. 8. Calculated temperature profiles for air side addition of ethanol. Also shown is estimated position of stagnation plane.

perature profile moves the flame region (i.e., region of appreciable flame radical concentration and high temperature) closer to the stagnation plane, and therefore closer to the region of maximum soot concentration, thereby increasing the rate of soot oxidation (see Figs. 8 and 9). Introduction of ethanol to the air stream moves the flame from a soot formation (SF) type toward a soot formation/oxidation (SFO) type, in which soot particles must travel a shorter distance into the oxidation region [14]. As more ethanol vapor is added to the air stream, the flame begins to transition to a multiple flame structure due to partial premixing as has been studied with other fuel-rich-oxidizer premixed flames [28].

To explore further the mechanism of particle reduction in these flames, Table 2 shows the stepwise

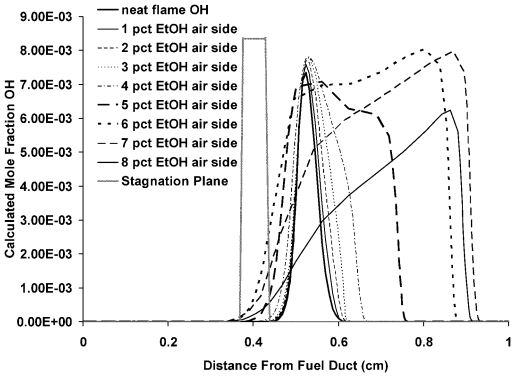

Fig. 9. Calculated OH profiles for air side addition of ethanol. Also shown is estimated position of stagnation plane.

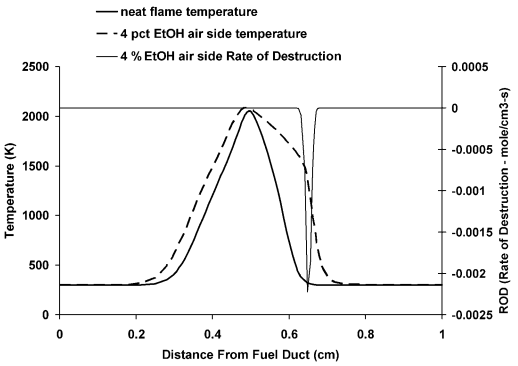

Fig. 10. Calculated temperature profile for air side addition of ethanol, overlaid with overall rate of destruction of ethanol vapor (4% mole fraction fuel side). Note the coincidence of ethanol vapor combustion with edge of broadened temperature profile.

reactions of ethanol added to the oxidizer stream predicted by the calculation for this flame system. This table shows the reaction of ethanol and air in the *premixed* region of the diffusion flame. This region is the region between the oxidizer duct and the diffusion flame zone, when there is ethanol vapor mixed in with the oxidizer gas. As in Table 1, species in bold face in the reaction list on the right side of Table 2 are the species for which the rates of destruction listed apply. Also shown is the temperature at which maximum rates of destruction (ROD) and rates of production (ROP) for several species occur. Table 2 shows that in the lean premixed flame region, the ethanol vapor is converted by a series of oxidation reactions (mainly involving H atom abstraction) to eventually yield OH and CO, prior to reaching the main combustion region of the diffusion flame (see Fig. 10). The OH and CO produced by the premixed ethanol/air flame are formed at a temperature near 1500 K, and are then convected into the diffusion flame combustion region.

Table 2
Reaction path of ethanol to products for ethylene/air opposed flow diffusion flames that have ethanol vapor added to the air side

Max. T (K) at peak		Air side ethanol addition to ethylene/air opposed flow flame
ROP	ROD	
	1500	**C2H5OH**
		32% 54% 8%
1500	1500	**CH3CHOH** **CH3CH2O** **C2H4OH**
		99% 49% 99%
1500	1500	**CH3HCO** **HOC2H4O2**
		74% 49% 99%
1500	1500	**CH2HCO** **CH2O**
		57% 99%
1500	1500	**CH2CO** **HCO**
		99% 66%
1500	1500	**HCCO** **HO2**
		99% 47%
1500		**CO** **OH**

C2H5OH + OH → CH3CH2O + H2O (39%)
C2H5OH + O → CH3CHOH + OH (16%)
C2H5OH + O → CH3CH2O + OH (16%)
C2H5OH + OH → CH3CHOH + H2O (16%)
C2H5OH + OH → C2H4OH + H2O (8%)

CH3CH2O + M → CH3HCO + H + M (49%)
CH3CH2O + M → CH3 + CH2O + M (49%)
CH3CHOH + O2 → CH3HCO + HO2 (98%)
C2H4OH + O2 → HOC2H4O2 (100%)

CH3HCO + OH → CH2HCO + H2O (43%)
CH3HCO + OH → CH3CO + H2O (5%)
CH3HCO + OH → CH3 + HCOOH (18%)
CH3HCO + O → CH2HCO + OH (9%)
CH3HCO + H → CH2HCO + H2 (22%)
HOC2H4O2 → CH2O + CH2O + OH (100%)

CH2HCO + O → CH2O + HCO (23%)
CH2HCO + OH → CH2CO + H2O (14%)
CH2HCO → CH2CO + H (43%)
CH2HCO → CH3 + CO (10%)
CH2O + H → HCO + H2 (18%)
CH2O + OH → HCO + H2O (71%)
CH2O + O → HCO + OH (10%)

CH2CO + H → HCCO + H2 (20%)
CH2CO + OH → HCCO + H20 (79%)
HCO + O2 → CO + HO2 (67%)
HCO + M → CO + H (32%)

HO2 + H → OH + OH (47%)
HO2 + OH → O2 + H2O (41%)
CH3 + HO2 → CH3O + OH (10%)
HCCO + O2 → OH + CO + CO (67%)
HCCO + O → H + CO + CO (20%)
HCCO + OH → C2O + H2O (12%)

Note. Important reactions contributing to each species concentration are shown to the right. Percentage value in parentheses refers to the amount of species in **bold** consumed or produced by that reaction.

The convection of the hot gases from the premixed flame into the diffusion flame region results in a preheating of the oxidizer side of the diffusion flame, raises peak flame temperature, and accounts for the broadened OH and temperature profiles in calculation and experiment (see Figs. 7–10).

Table 3 shows the calculated peak temperatures, calculated peak mole fractions, and integrated calculated mole fractions for several species identified as important for soot formation in Tables 1 and 2, as ethanol addition to the oxidizer gas is varied up to 4% mole fraction. The table shows calculated values for air side ethanol addition up to 4%. Calculations beyond 4% used relaxed convergence criteria, as noted earlier (only for air side addition). The integration of mole fraction was performed using Simpsons Rule [29] and extended over the full space between oxidizer and flame ducts. It appears that the observed and calculated decrease in soot and soot precursor concentration is due mainly to a combination of increased radical concentration and thermal effect caused by the preheating of the oxidizer gases occurring in the premixed part of the flame, raising calculated peak flame temperature (33 K, or 1.6%). Peak calculated mole fractions for all species in Table 3 that are important for soot formation decrease, while the integrated calculated mole fractions for the flame propagating species H, O, and OH increase by 41, 52, and 142%, respectively. The effect of increased flame temperature on radical species concentrations is complicated by the accompanying broadening of the temperature profile. However, we believe the increase in OH integrated mole fraction as ethanol addition increases is indicative of a thermal effect on the net rate constant for OH formation. In addition to decreasing soot by increasing OH and increasing direct oxidation (see

Table 3
The calculated change in peak and integrated mole fraction for air side ethanol addition for H, O, OH, CH_2, C_2H_2, C_3H_3, n-C_4H_5, C_4H_6, A1, and A4

Mole fraction EtOH	T (K)	Peak mole fraction; integrated mole fraction (mole fraction-cm)									
		H ($\times 10^{-4}$)	O ($\times 10^{-4}$)	OH ($\times 10^{-4}$)	CH_2 ($\times 10^{-6}$)	C_2H_2 ($\times 10^{-2}$)	C_3H_3 ($\times 10^{-6}$)	n-C_4H_5 ($\times 10^{-8}$)	C_4H_6 ($\times 10^{-4}$)	A1 ($\times 10^{-5}$)	A4 ($\times 10^{-9}$)
0	2053	65; 3.97	52; 2.7	74; 3.93	57; 1.46	5.5; 0.651	104; 7.7	51; 2.39	27; 2.30	14; 1.44	25; 2.48
1	2058	62; 4.20	47; 2.8	76; 4.58	52; 1.44	5.4; 0.655	97; 7.4	47; 2.27	27; 2.25	13; 1.35	19; 1.98
2	2062	59; 4.40	44; 3.0	77; 5.41	47; 1.40	5.3; 0.658	90; 7.1	45; 2.14	27; 2.24	12; 1.25	15; 1.54
3	2068	54; 4.80	39; 3.3	77; 6.62	41; 1.38	5.2; 0.660	82; 6.8	40; 2.01	26; 2.24	11; 1.15	11; 1.14
4	2086	48; 5.60	32; 4.1	78; 9.50	35; 1.40	5.0; 0.670	75; 6.5	36; 1.87	26; 2.27	9; 1.03	7; 0.75
% change	+1.6 (33 K)	−26; +41	−63; +52	+5.4; +142	−38; −4	−9; +3	−28; −16	−29; −22	−4; −1	−33; −28	−72; −70

Note. This table is presented to show that most species influencing A1 and A4 production are affected by air side addition of ethanol vapor.

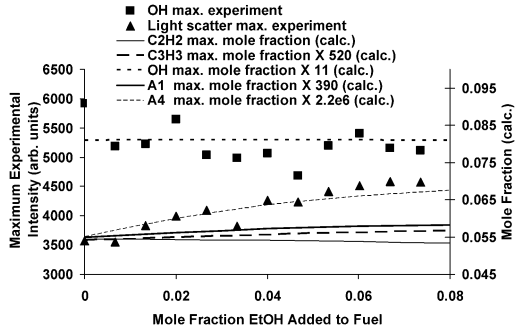

Fig. 11. Graph of experimental measurements and predictions based upon calculations for OH, soot, and soot precursors, for fuel side addition of ethanol.

(R8)), the thermal effect decreases A1–A4 formation by increasing integrated OH and H mole fraction, decreasing the amount of CH_2 available for reaction to propargyl. Formation of propargyl (C_3H_3) is dependent upon the reaction:

$$CH_2 + C_2H_2 \rightarrow C_3H_3 + H. \quad \text{(R9)}$$

The rate of production of propargyl by this reaction decreases approximately 28% when the oxidizer contains 4% mole fraction ethanol.

4.3. Fuel side addition

In experiments and calculations, fuel side addition of ethanol increases soot and soot precursors, while peak OH concentrations remain approximately constant. A graph of experimental measurements of peak light scatter and OH fluorescence and predictions of species maximum mole fraction based on calculations, for fuel side addition of ethanol, is shown in Fig. 11. The calculated data have been normalized to the experimental data to allow comparisons of the trends shown by each. As in Fig. 6, the error in the measured scattered laser intensity and OH fluorescence is estimated to be approximately 5%, based upon pixel to pixel noise in the individual images. Overall, the trend of the change (increasing), with increasing fuel side ethanol addition, of calculated peak mole fractions for the species A1–A4 is in good agreement with peak experimental values (measured along the centerline between burner ducts) of light scatter, while the change, with increasing fuel side ethanol addition, of the calculated peak mole fraction of OH is in reasonable agreement with peak measured values of OH fluorescence. Calculation and experimental measurement show peak OH concentration to remain nearly constant with increasing ethanol addition. For these flames, the calculation was able to reach convergence for all mole fractions of ethanol using an initial grid of 60 points. Individual experi-

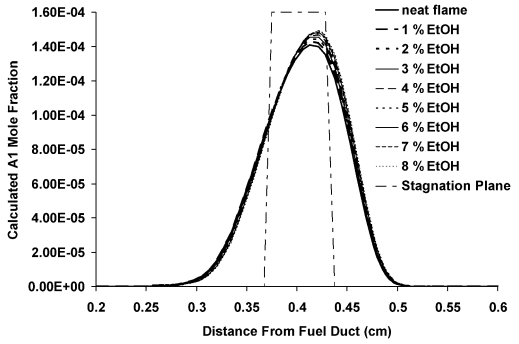

(a)

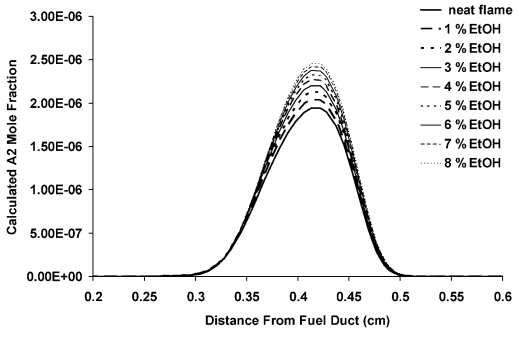

(b)

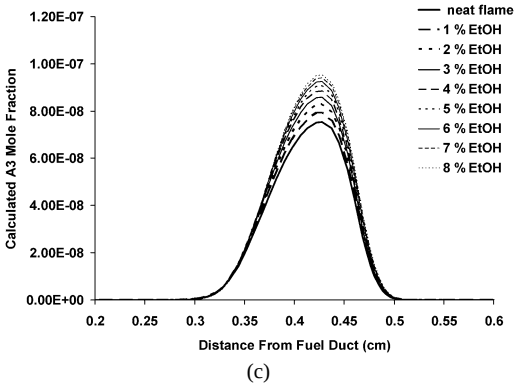

(c)

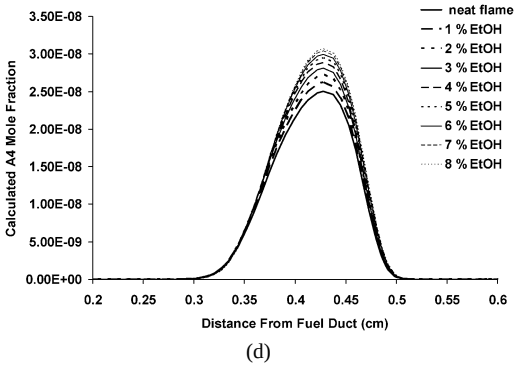

(d)

Fig. 12. Calculated A1 (a), A2 (b), A3 (c), and A4 (d) mole fraction profiles for increasing amounts of ethanol vapor added to the fuel stream.

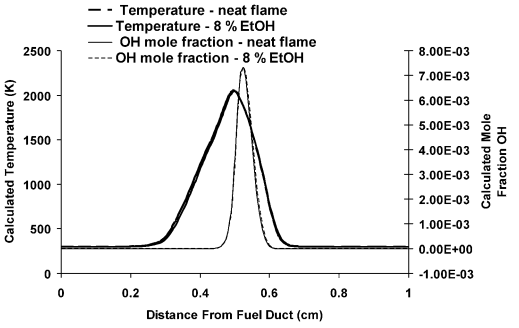

Fig. 13. Calculated temperature and OH profiles for neat flames and for flames with 8% ethanol vapor added to the fuel stream. Intermediate values of ethanol addition yield temperatures and OH profiles between those for the extreme values. Note that the calculation predicts negligible change in OH and temperature for fuel side addition of ethanol.

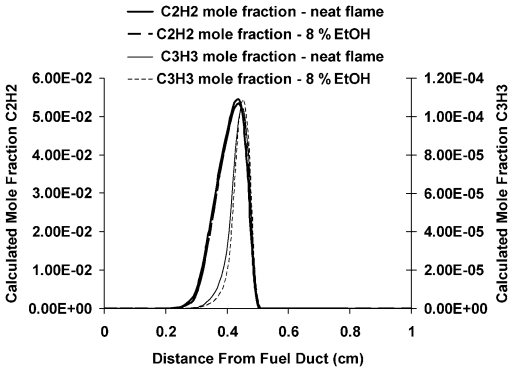

Fig. 14. Calculated acetylene (C_2H_2) and propargyl (C_3H_3) profiles for increasing amounts of ethanol vapor added to the fuel stream. Note that the calculation predicts negligible change in acetylene and very small decrease in propargyl for fuel side addition of ethanol.

mental images do not show apparent differences and are not reproduced here.

Calculations predict that addition of 8 mol% ethanol to the fuel stream increases the integrated mole fraction of aromatic species A1 (C_6H_6), A2 ($C_{10}H_8$), A3 ($C_{14}H_{10}$), and A4 ($C_{16}H_{10}$) by approximately 3, 19, 23, and 22%, respectively (see Figs. 12a–12d). The peak increase in light scatter observed experimentally was approximately 19%. Temperature and OH concentration are predicted by calculation to remain approximately constant (see Fig. 13). Acetylene is predicted to remain approximately constant while propargyl concentration is predicted to decrease approximately 9% when 8% ethanol is added to the fuel stream (Fig. 14). In what follows, the production of soot precursors is divided into a discussion of A1 formation followed by a discussion of A2–A4 formation.

Table 4
Reaction path of ethanol to products for ethylene/air opposed flow diffusion flames that have ethanol vapor added to the fuel side

Max. T (K) at peak		Fuel side ethanol addition to ethylene/air opposed flow flame
ROP	ROD	
	1500	C2H5OH
		58% 30% 8%
1500	1550	C2H4 CH2OH C2H5
		99% 78% 21%
1550		Same as neat fuel C2H6
1500	1500	CH2O CH3
		99% 60% 30%
1500	1500	HCO CH4 C2H3
		94% 94% 5% CH3 90%
1500	1500	CO CH3CHO C3H4 C4H6
		99% 85%
1500	1550	CH3CO C3H3 C4H5
		97% C4H4
		4% 2.5% 1% C6H6
		52% A1
1550		

C2H5OH (+M) → C2H4 + H2O (+M) (58%)
C2H5OH (+M) → CH3 + CH2OH (+M) (30%)
C2H5OH (+M) → C2H5 + OH (+M) (8%)

CH2OH (+M) → CH2O + H (+M) (98%)
CH2OH + H → CH20 + H2 (1%)
C2H5 + H → CH3 + CH3 (78%)
C2H5 + H2 → C2H6 + H (21%)

CH3 + H2 → CH4 + H (60%)
CH3 + C2H4 → C2H3 + CH4 (30%)
CH2O + H → HCO + H2 (99%)

HCO + C3H3 → aC3H4 + CO (47%)
HCO + C3H3 → pC3H4 + CO (47%)
HCO + CH3 → CH3CHO (5%)
C2H3 + C2H4 → C4H6 + H (85%)
C2H3 + C2H3 → C4H6 (5%)

aC3H4 + H → C3H3 + H2 (99%)
pC3H4 + H → C3H3 + H2 (99%)
C4H6 + H → n-C4H5 + H2 (33%)
C4H6 + H → i-C4H5 + H2 (52%)

C4H5 → C4H4 + H (97%)
C4H5 + C2H2 → A1 + H (2.5%)
C3H3 + C3H3 → A1 (5%)
C6H6 + H → A1 + H (52%)

Note. Important reactions contributing to each species concentration are shown to the right. Percentage value in parentheses refers to the amount of species in **bold** consumed or produced by that reaction.

4.3.1. A1 formation

Because the calculated change in propargyl mole fraction with ethanol addition was in the opposite direction of the change in A1 mole fraction for fuel side ethanol addition, a calculation of rate of formation of A1 by reaction was performed. The reactions contributing to A1 formation, and the change in A1 rate of formation per reaction, relative to the neat flame, when 8% ethanol was added to the fuel stream, are as follows:

Reaction	Calculated change in rate of A1 formation—8% EtOH addition to fuel (relative to neat flame)
$C_3H_3 + C_3H_3 \rightarrow A1$	−8% (R4)
$n\text{-}C_4H_5 + C_2H_2 \rightarrow A1 + H$	23% (R5)
$l\text{-}C_6H_6 + H \rightarrow A1 + H$	27% (R6)
$n\text{-}C_6H_7 \rightarrow A1 + H$	34% (R7)

The calculation predicts that all of the increase in A1 produced by fuel side ethanol addition is caused by reactions other than propargyl recombination. The reactions of phenyl (A1•) influencing A1 formation,

$$A1\bullet + H\,(+M) \rightarrow A1\,(+M), \qquad \text{(R10)}$$

$$A1 + OH \rightarrow A1\bullet + H_2O, \qquad \text{(R11)}$$

are included in the mechanism but are not considered important here for A1 formation because the change in rate of each was less than 1% with fuel side ethanol addition.

To understand why propargyl is decreased, and why (R5)–(R7) are enhanced, it is necessary to track the path of oxygen and carbon added, via ethanol, to the fuel gas. A listing of the reactions responsible for the increase in soot formation for fuel side ethanol addition, predicted by the calculations, may be found in Table 4. The initial decomposition reactions for ethanol when added on the fuel side of the flame differ from those for air side ethanol addition (see Table 2). For fuel side addition, in the absence of oxygen, ethanol decomposition occurs via a pyrolysis mechanism at approximately 1500 K:

$$C_2H_5OH\,(+M) \rightarrow C_2H_4 + H_2O\,(+M) \quad 58\%, \qquad \text{(R12)}$$

$$C_2H_5OH\,(+M) \rightarrow CH_3 + CH_2OH\,(+M) \quad 30\%, \qquad \text{(R13)}$$

$$C_2H_5OH\,(+M) \rightarrow C_2H_5 + OH\,(+M) \quad 8\%. \qquad \text{(R14)}$$

The ethylene, water, ethyl radical, and OH radical formed from the initial decomposition have little additional effect on the chemistry as they are very slight perturbations on the concentrations of these species relative to the neat flame (see Figs. 13 and 14) or are similar to fuel or initial fuel decomposition products. The bulk of the reactive oxygen (as CH_2OH) is stepwise-converted to HCO, which then reacts with propargyl to yield CO and C_3H_4, which is then near quantitatively reconverted to propargyl. The increase in other soot precursors [6] predicted by the calculation may be ascribed to introduction of methyl radical (R13) into a relatively low-temperature hydrocarbon/acetylene bath [14].

The methyl radicals formed in cooler regions of the flame (1400–1700 K) via ethylene pyrolysis react with propargyl (C_3H_3) to form C_4H_6:

$$C_3H_3 + CH_3\,(+M) \rightarrow C_4H_6\,(+M). \qquad \text{(R15)}$$

This reaction shows a calculated increase in the rate of production of C_4H_6 of 17% for the flame with 8 mol% fraction ethanol compared to the neat ethylene/air flame. Mole fraction profiles (see Fig. 14) of propargyl show a slight decrease in concentration over this temperature range (1400–1700 K). Approximately 85% of the C_4H_6 reacts with H to form C_4H_5,

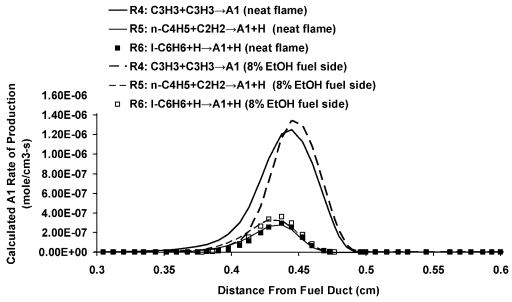

Fig. 15. Rates of production of A1 by the three most important reactions contributing to A1 production. Note the enhancement of rates of reactions that do not involve propargyl.

which then reacts in the acetylene bath to form A1 and aromatic precursors.

$$C_4H_6 + H \rightarrow C_4H_5 + H_2, \qquad \text{(R16)}$$

$$C_4H_5 + C_2H_2 \rightarrow A1 + H, \qquad \text{(R17)}$$

$$C_4H_5 + C_2H_2 \rightarrow n\text{-}C_6H_7. \qquad \text{(R18)}$$

Overall, the calculation predicts that the addition of ethanol to the fuel stream has a negative effect on integrated C_3H_3 concentration while enhancing alternate pathways, via C_4H_6 production, to formation of initial aromatic ring species (see Fig. 15). This result was not anticipated prior to the experimental studies. However, it should be noted that other researchers [9] have measured soot increases during combustion of ethanol/hydrocarbon mixtures, relative to neat ethylene combustion. Increases in soot precursor production have also been reported for methane addition to heptane/air flames [30].

4.3.2. A2–A4 formation

For fuel side ethanol addition, the calculation predicts an increase in integrated mole fraction of benzene of 3% when 8% ethanol is added, relative to the neat flame. For the same comparison, the predicted increase in A2 (naphthalene), A3 (phenanthrene), and A4 (pyrene) is 19, 23, and 22%, respectively (see Figs. 12a–12d). However, the absolute change in mole fraction of A1 with 8% fuel side ethanol addition is greater than 10 times the absolute change in A2 addition. The change in mole fraction in going from the neat flame to the flame with 8% ethanol added to the fuel side for A1, A2, A3, and A4 is 5×10^{-7}, 4.2×10^{-8}, 1.6×10^{-9}, and 4.8×10^{-10}, respectively. In contrast to the reaction path to A1 formation discussed above, the formation of A2–A4 follows the H-abstraction–C_2H_2-addition mechanism [31]. For A1 conversion to A2, an example of one of the path-

ways may be summarized as follows:

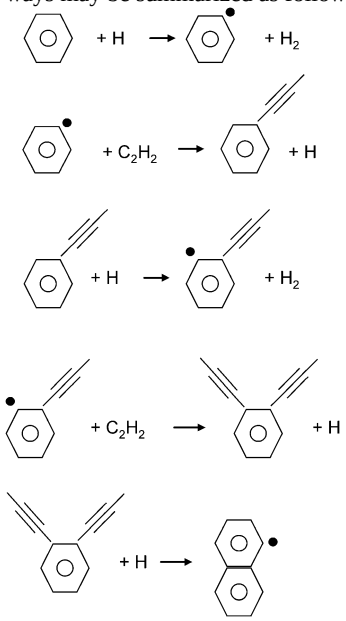

5. Conclusion

This study provides an example of how soot formation in opposed flow ethylene/air diffusion flames is dependent upon temperature, flame radical, and bath gas compositions. Differing chemical behavior in opposed flow flames depending on fuel or air side addition of ethanol vapor has been observed experimentally and modeled, and shown to occur via different pathways within the context of a detailed chemical mechanism. In particular, ethanol introduced into the air side of the flame creates a premixed combustion (secondary flame zone) region prior to the main diffusion flame region. Hot gas products from this premixed flame region, including OH, are convected into the diffusion flame zone, increasing peak temperature and broadening the OH concentration profile. The broadened OH concentration profile moves the oxidizing region of the flame closer to the stagnation plane and to the high soot concentration region of the flame. The increased temperature and integrated OH mole fraction cause an increase in soot and soot-precursor oxidation, leading to lower overall soot concentrations in ethylene/air diffusion flames with ethanol added to the air stream. It should be noted that the effect of radiation from soot in the experiment was not accounted for in the "particle-free" computational model.

When ethanol is introduced into the fuel stream of the ethanol/air opposed flow diffusion flame, initial decomposition of ethanol occurs via pyrolysis reactions because of the lack of oxygen in the fuel stream. Methyl radical produced during the initial steps of decomposition of ethanol reacts with propargyl to produce C_4H_6, which leads to increased production of A1.

In summary, we believe that the addition of ethanol to the air side of the ethylene/air diffusion flame decreases soot concentration mainly through a thermal mechanism. This is supported by observation of the flame and the calculated increase in temperature (33 K) and increase in OH concentration (142%) relative to the neat flame. Addition of ethanol to the fuel side of the ethylene/air diffusion flame increases soot mainly through a chemical mechanism involving introduction of methyl radical into an ethylene/acetylene bath. This is supported by observation of the flame and the calculated constant temperature and OH concentrations over the studied range of ethanol addition.

Acknowledgments

Funding support for this work was provided by the U.S. DoD Strategic Environmental Research and Development Program (SERDP). The authors thank Michael Frenklach and Charles Westbrook for much of the chemical mechanism used in the calculations. Also, the authors thank Sukh Sidhu, Med Colket, Valeri Babushok, and William Anderson for helpful discussions.

References

[1] R.P. Howard, Experimental Characterization of Gas Turbine Emissions at Simulated Altitude Conditions, September 1996, AEDC-TR-96-3.
[2] D.W. Dockery, C.A. Pope, X. Xu, J.D. Spengler, J.H. Ware, M.E. Fay, B.G. Ferris, F.E. Speizer, N. Engl. J. Med. 329 (1993) 1753–1759.
[3] M.F. Denisenko, A. Pao, M.-S. Tang, G.P. Pfeifer, Science 273 (1996) 430–432.
[4] R. Niedzwiecki, Aircraft Technology and its Relation to Emissions, Report of The Intergovernmental Panel on Climate Change, IPCC, chap. 7, in press.
[5] Reduced PM2.5 Emissions for Military Gas Turbine Engines Using Fuel Additives, administered by the Strategic Environmental Research and Development Program (DoD, EPA, DOE).
[6] H. Richter, J.B. Howard, Progr. Energy Combust. Sci. 26 (2000) 565–608.
[7] M.B. Colket, R.J. Hall, in: H. Bockhorn (Ed.), Soot Formation in Combustion, Springer-Verlag, Berlin, 1994, p. 417.
[8] I. Glassman, Combustion, second ed., Academic Press, San Diego, 1987, pp. 360–375.
[9] A. Alexiou, A. Williams, Combust. Flame 104 (1996) 51–65.

[10] J. Appel, H. Bockhorn, M.Y. Frenklach, Hydrocarbons Combust. Flame 121 (2000) 122–136.
[11] R.J. Hall, M.D. Smooke, M.B. Colket, in: F.L. Dryer, R.F. Sawyer (Eds.), Physical and Chemical Aspects of Combustion—A Tribute to Irvin Glassman, Gordon and Breach, New York, 1997, pp. 189–230.
[12] E.J. Welle, W.L. Roberts, C.D. Careter, J.M. Donbar, Combust. Flame 135 (2003) 285–297.
[13] C.R. Shaddix, K.C. Smyth, Combust. Flame 107 (1996) 418–452.
[14] J.Y. Hwang, S.H. Chung, Combust. Flame 125 (2001) 752–762.
[15] M.D. Rumminger, G.T. Linteris, Combust. Flame 128 (2002) 145–164.
[16] D.X. Du, H. Wang, C.K. Law, Combust. Flame 113 (1988) 264–270.
[17] A.M. Lentati, H.K. Chelliah, Combust. Flame 115 (1998) 158–179.
[18] I.M. Kennedy, Combust. Sci. Technol. 59 (107) (1988) 1.
[19] K.C. Smyth, C.R. Shaddix, D.A. Everest, Combust. Flame 111 (1997) 185–207.
[20] J.B. Howard, W.J. Kausch, Progr. Energy Combust. Sci. 6 (1980) 263–276.
[21] K.T. Kang, J.Y. Hwang, S.H. Chung, Combust. Flame 109 (1997) 266–281.
[22] P.C. Reist, Aerosol Science and Technology, second ed., McGraw–Hill, New York, 1993, pp. 263–275.
[23] K.H. Song, P. Nag, T.A. Litzinger, D.C. Haworth, Combust. Flame 135 (2003) 341–349.
[24] H.F. Calcote, Combust. Flame 42 (1981) 215–242.
[25] B.S. Haynes, H.G. Wagner, Progr. Energy Combust. Sci. 7 (1981) 229–273.
[26] C.J. Sung, J.S. Kistler, M. Nishioka, C.K. Law, Combust. Flame 105 (1996) 189–201.
[27] C.R. Shaddix, J.E. Harrington, K.C. Smyth, Combust. Flame 99 (1994) 723–732.
[28] R.D. Lockett, B. Boulanger, S.C. Harding, D.A. Greenhalgh, Combust. Flame 119 (1999) 109–120.
[29] M. Abramowitz, I.A. Stegun (Eds.), Handbook of Mathematical Functions with Formulas, Graphs, and Mathematical Tables, ninth ed., Dover, New York, 1972, p. 886.
[30] J.F. Roesler, S. Martinot, C.S. McEnally, L.D. Pfefferle, J.-L. Delfau, C. Vovelle, Combust. Flame 134 (2003) 249–260.
[31] H. Wang, M. Frenklach, Combust. Flame 110 (1997) 173–221.